J Biomol NMR (2012) 53:161–165
DOI 10.1007/s10858-012-9633-6

NMR STRUCTURE NOTE

NMR structure note: the ferrous iron transport protein C (FeoC) from *Klebsiella pneumoniae*

Kuo-Wei Hung · Tzu-hsuan Juan · Yen-lan Hsu · Tai Huang Huang

Received: 29 March 2012 / Accepted: 27 April 2012 / Published online: 13 May 2012

Biological context

Iron is an essential nutrient involved in many important biological processes ranging from electron transfer, oxygen transport, gene regulation, photosynthesis, N_2 fixation to DNA biosynthesis (Andrews et al. 2003). Thus, the ability to acquire sufficient quantities of iron from the environment is vital for the survival of living organisms. This is particularly true for pathogens that must compete with the host iron-withdrawal response for their iron supplies. However, iron is also toxic and excess iron can be detrimental for the living system (Touati 2000). It is, therefore, essential for almost all life forms to maintain proper iron homeostasis (Andrews et al. 2003).

Feo is a unique ferrous iron transporter commonly utilized by bacterial systems for acquiring ferrous iron from the environment (Cartron et al. 2006). It was first discovered in *Escherichia coli* K-12 (Hantke 1987). Subsequently the *feo* locus was cloned and sequenced (Kammler et al. 1993). The importance of the Feo system has been confirmed in several systems. Both *E. coli* and *Salmonella feoB* mutants are attenuated in their abilities to colonize the mouse intestine presumably due to their inability to transport ferrous iron within the anaerobic environment of the mouse intestine (Stojiljkovic et al. 1993; Tsolis et al. 1996). In *H. pylori*, FeoB appears to provide the main route of iron uptake. It is required for *H. pylori* colonization of mouse gastric mucosa, as well as for normal growth and iron-uptake under iron restricted conditions (Velayudhan et al. 2000). FeoB is also required for intracellular growth of *Legionella pneumophila* (Robey and Cianciotto 2002). Thus, various studies have clearly established an in vivo role for Feo in colonization of the gut and in virulence.

The *feo* operon of enterobacteria encodes three proteins: FeoA, FeoB and FeoC. FeoA is a small SH3-like protein predicted to act as GTPase activating protein (GAP) and/or Fe-dependent repressor (Cartron et al. 2006). FeoB is a large protein (773 a.a.) composing of a 270-residue cytosolic N-terminal domain (NFeoB, residues 1–270) that contains a G-protein domain (a.a. 1–170) and a helical bundle S-domain (a.a. 171–270) presumed to be a GDP-dissociation inhibitor (GDI). The C-terminal region of FeoB is a helical transmembrane domain which is likely to act as the ferrous iron permease and essential for ferrous iron transport activity. FeoC (also called yhgG) is a small 78-residue, hydrophilic winged-helix domain (WHD) found only in γ-proteobacteria. The *feo*C gene was found preceding the *feo*B gene in the *feo* operon. Multiple sequence alignment of FeoC proteins shows that they possess four conserved cysteine residues ($CxxGxCKxCPx_{4\text{-}7}C$) that are likely to provide a binding site for an [Fe–S]-cluster. Thus, FeoC is presumed to be a [Fe–S]-dependent transcriptional regulator directly controlling the expression of the *feo* operon (Cartron et al. 2006).

Given its importance and novelty, there has had increasing interest in dissecting the molecular basis of the Feo system. In particular, the presence of a G-protein motif in the intracellular domain of FeoB (NFeoB) has spurred considerable interest in understanding its molecular basis and the structures of NFeoB from several species have

K.-W. Hung · T. Juan · Y. Hsu · T. H. Huang (✉)
Institute of Biomedical Sciences, Academia Sinica, Taipei, Taiwan, ROC
e-mail: bmthh@ibms.sinica.edu.tw

T. H. Huang
Genomics Research Center, Academia Sinica, Taipei, Taiwan, ROC

T. H. Huang
Department of Physics, National Taiwan Normal University, Taipei, Taiwan, ROC

been published within the last year (Guilfoyle et al. 2009; Hung et al. 2010). We have also determined the structures of NFeB from *K. pneumoniae* (*kp*NFeoB) and *Pyrococcus furiosus* (*pf*NFeoB) with and without bound ligands (Hung et al. 2010). The NFeoB from *E. coli* (*ec*NFeoB) was proposed to form a trimer with the center forming the cation binding site and the GDI domain working as a switch to control the cation transport (Guilfoyle et al. 2009). However, no Fe^{2+} binding was detected, probably due to difficulty of growing crystals of the FeoB/Fe^{2+} complex since Fe^{2+} is readily oxidized to Fe^{3+} which is insoluble. Furthermore, no interaction among the three Feo components has been reported and no information on the role of FeoA and FeoC is available. Here we report the solution NMR structure *Klebsiella pneumoniae* FeoC (*kp*FeoC) and discuss its possible functional roles.

Methods and results

Protein expression and purification

Isotopically labeled *kp*FeoC proteins were overexpressed in *E. coli* as GST fusion proteins and purified through Glutathione Sepharose 4B column (GE). The GST-tag was removed by PreScission Protease and *kp*FeoC was eluted from GST-affinity column. The protein was further purified through a HiLoad 16/60 Superdex 75 column. The purified protein contains 5 extra residues (GPLGS) at the N-terminus with a total length of 83 residues. The purity of the protein products were checked by SDS-PAGE and confirmed by mass spectrometry.

NMR spectroscopy

NMR spectra were acquired at 15 °C on Bruker Avance 500 and 600 MHz spectrometers equipped with triple resonance cryogenic probes. Samples for NMR experiments contain 0.2–1.0 mM protein in 20 mM phosphate buffer (pH 6.5), 50 mM NaCl, 0 (oxidized) or 10 mM (reduced) DTT and 10 % D2O. Sequence specific assignments of the polypeptide backbone were made from analysis of HNCA, HN(CO)CA, HNCO, HN(CA)CO, CBCA(CO)NH and HNCACB spectra. Side chain resonances were assigned from the combined information content of the ^{15}N-edited NOESY-HSQC, ^{13}C-edited NOESY-HSQC, HCCH-TOCSY and HBHA(CO)NH spectra. ^{1}H chemical shifts were externally referenced to 0 ppm methyl resonance of the 2,2-dimethyl-2-silapentane-5-

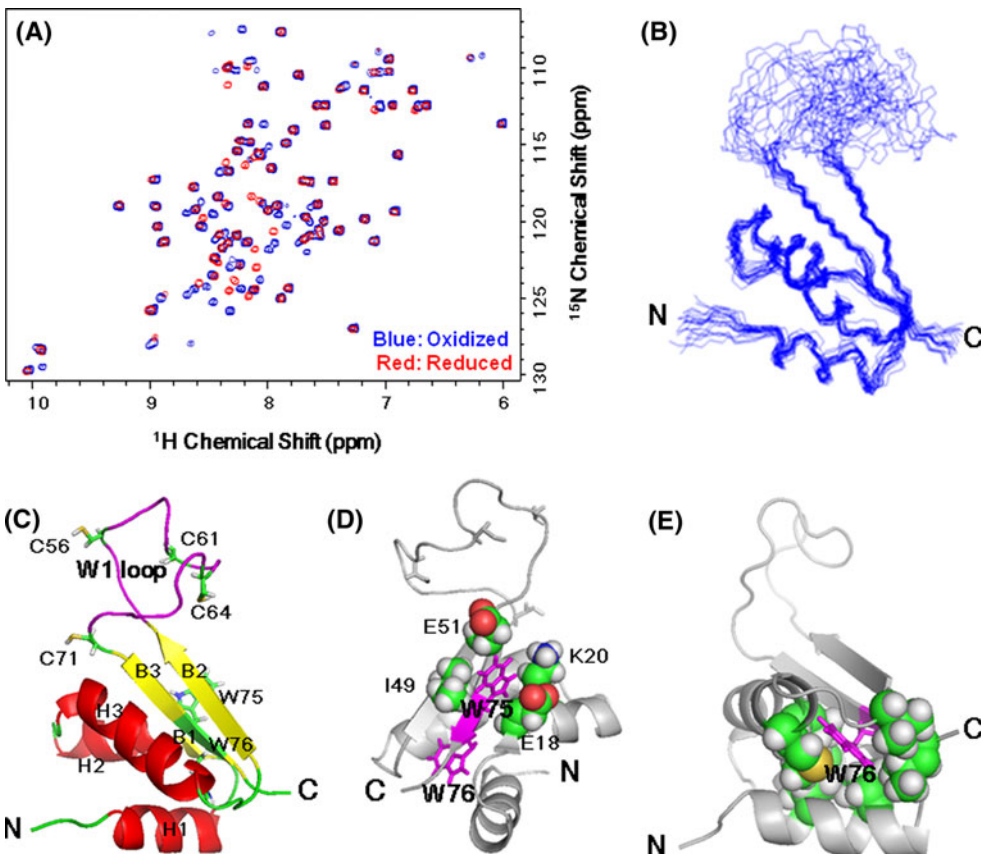

Fig. 1 **a** ^{1}H-^{15}N HSQC spectra of 0.5 mM of recombinant oxidized- (*blue*) and reduced- (*red*) *Kp*FeoC acquired at 288 K, pH6.5. The reduced spectrum was obtained in the presence of 10 mM DTT. **b** Overlay of the backbone traces of 20 best NMR structures. **c** Ribbon representation of the tertiary structure of *Kp*FeoC$_R$. The secondary structure elements and the four cysteine residues shown in sticks in W1 loop are labeled. The side chain of Trp^{75} was shown in sticks. **d** The spatial localization of Trp^{75} and Trp^{76} (Magenta). The side chain of Trp^{75} and Trp^{76} (behind B2 strand) are shown in sticks. **e** The hydrophobic core of *kp*FeoC. Trp^{76} (Magenta) is located at the center of the hydrophobic core

sulfonate, whereas ^{13}C and ^{15}N chemical shifts were indirectly referenced according to the IUPAC recommendations (Markley et al. 1998). NMR data were processed using software Topspin and analyzed by software SPARKY (T. D. Goddard and D. G. Kneller, SPARKY 3, University of California, San Francisco, CA, USA).

NOE distance constraints were obtained from ^{15}N-edited NOESY-HSQC and ^{13}C-edited NOESY-HSQC spectra. The dihedral angle restraints on phi torsion angles (ϕ) and psi torsion angles (ψ) of the protein backbone were empirically predicted using the TALOS software program (Cornilescu et al. 1999). Hydrogen bonds derived from CSI prediction (Wishart and Sykes 1994) were introduced as a pair of distance restraints. Families of structures were calculated by a simulated annealing (SA) approach followed by a refinement procedure using software ARIA 1.2 (Linge et al. 2001). Energy minimization was carried out using torsion angle dynamics (TAD). PARALLHDG force field was employed as non-bonded interactions for the structure calculation. In the first ARIA round, manually-assigned NOEs were included for the generation of initial-folded structures. The unambiguous and ambiguous NOE restraints derived from ARIA outputs were further analyzed and employed as inputs for the next round of calculations. Slightly modified slow-cooling standard SA protocols were used for the calculations. The quality of the constraints was checked by analyzing the violations of the calculated conformers using MolMol (Koradi et al. 1996) and Procheck (Laskowski et al. 1996) software programs.

NMR resonance assignments and structure determination of kpFeoC$_R$

The purified recombinant *kp*FeoC protein exists as a monomer in solution over a wide range of pH conditions, as monitored by size-exclusion chromatography (pH 6.5–8.5). The well-dispersed ^{1}H-^{15}N HSQC spectra of *kp*FeoC contain many peaks beyond 8.5 ppm in the ^{1}H dimension, indicating that *kp*FeoC is well-structured (blue peaks in Fig. 1a). Addition of 10 mM dithiothreitol (DTT) to the sample to reduce the four cysteine residues (Cys^{56}, Cys^{61}, Cys^{64} and Cys^{71}) resulted in the disappearance of a set of resonances and the appearance of a new set of resonances in the 8.0–8.8 ppm region. The ^{1}H, ^{15}N and ^{13}C resonances of the DTT-reduced *kp*FeoC (*kp*FeoC$_R$) at pH 6.5, 288 K have been completely assigned using standard multidimensional heteronuclear NMR techniques (Deposited in the BioMagResBank under accession number 15634). The backbone ^{1}H, ^{15}N and ^{13}C resonances of the non-reduced *kp*FeoC at pH 6.5, 288 K have also been assigned. The results showed that the loop region exists in a mixture of two conformers, as indicated by the presence of two sets of resonances, presumably due to the presence of mixed oxidation/disulfide states. The secondary structure of *kp*FeoC$_R$, deduced from the consensus chemical shift index (Wishart and Sykes 1994), comprises of three helices (H1, a.a. 4–13; H2, a.a. 19–25; and H3, a.a. 33–42) and three β-strands (B1, a.a. 16–18; B2, a.a. 46–52; and B3, a.a. 73–77) in a H1-B1-H2-H3-B2-B3 topology.

The solution structure of *kp*FeoC$_R$ was further computed based on distance geometry calculations and energy minimization with 1,198 experimental and empirical NMR restraints including 1,075 NOE restraints, 23 hydrogen bond restraints and 100 dihedral angle restraints. Figure 1b shows an overlay of the backbone traces of an ensemble of 20 structures (selected from a set of 100 structures) with lowest energies and good agreement with NMR restraints. A summary of the structure statistics for these 20 structures is given in Table 1. The root-mean-square-deviation (RMSD) values of these structures were 0.436 ± 0.083 Å and 2.468 ± 0.518 Å for the backbone atoms of the

Table 1 Structural statistics of *kp*FeoC$_R$

No. of NMR constraints	
Intra-residues	566
Sequential (|i–j = 1|)	259
Medium range (|i–j = 4|)	99
Long range (|i–j ≥ 5|)	151
Hydrogen bond constraints	23
Dihedral angle constraints	100
X-PLOR energies (kcal mol^{-1})[a]	
E_{total}	−2,134.14 ± − 75.31
E_{bond}	1.18 ± 0.08
E_{angle}	27.35 ± 0.55
E_{impr}	1.54 ± 0.15
E_{dihed}	354.98 ± 2.34
E_{vdw}	−141.66 ± 14.85
E_{elec}	−2,377.52 ± − 71.06
R.M.S.D. from experimental constraints	
Distances (Å)	0.001 ± 0.000
Dihedral angles (°)	0.280 ± 0.002
R.M.S.D. for structured region (Å) (for backbone)	0.436 ± 0.083
R.M.S.D. for structured region (Å) (for heavy atoms)	1.091 ± 0.079
R.M.S.D. for the whole protein (Å) (for backbone)	2.468 ± 0.518
R.M.S.D. for the whole protein (Å) (for heavy atoms)	2.618 ± 0.411
Ramachandran parameter (%)	
Most favored region	82.6
Additionally allowed	14.5
Generously allowed	2.9
Disallowed	0.0

[a] There are no violations observed for the distance and angle restraints of refined structures

structured regions and the full length protein, respectively. The large RMSD of the full length protein is mainly due to the poorly defined long W1 loop. The Ramachandran plot analysis indicated that 82.6 % of residues are in the most favored region, 14.5 % in the additionally allowed region, 2.9 % in the generously allowed region and 0.0 % of residues are in the disallowed regions. The experimental constraints and the coordinates of 20 best conformers of *kp*FeoC$_R$ have been deposited in Protein Data Bank (PDB ID: 2K02).

Overview of the structural of kpFeoC$_R$

The solution structure of *kp*FeoC$_R$ protein comprises a three-helix bundle packed against a three-strand anti-parallel β-sheet (Fig. 1c). The B2-B3 strands are connected by a 20-residue long loop (W1 loop). The Trp^{76} residue, which is conserved in all prokaryotes characterized to date except in *Yesinia enterocolitica* where it is replaced by a tyrosine residue, is located in the middle of a hydrophobic core composing of Val^{7}, Leu^{11}, Ala^{19}, Ile^{33}, Met^{36}, Leu^{37}, Met^{40}, Val^{46} and Leu^{78} (Fig. 1d). Whilst the side chain of the adjacent Trp^{75} residue, which is conserved in most prokaryotes characterized to date but is replaced by a valine in *Cronobacter turicensis* and a isoleucine in *Yesinia enterocolitica* sticks out to the solvent accessible surface and interacts with side chains of Glu^{18}, Lys^{20}, Ile^{49} and Glu^{51}. These two terminal tryptophan residues likely play an important structural role in the folding of *kp*FeoC$_R$.

The coordinates of the solution structure of the reduced FeoC from *E. coli* (*ec*FeoC) has been deposited in PDB data bank (PDB ID: 1XN7). However, the oxidation state of *ec*FeoC is not specified. The *kp*FeoC$_R$ is highly homologous to *ec*FeoC (72 % identity), thus their structures are also very similar (Fig. 2a). The RMSD of the N-terminal 42 residues encompassing the helical bundle region of these two proteins is 1.627 Å. However, *kp*FeoC$_R$ has much more compact β-sheet structure with well-defined β strands whilst the B2–B3 region of *ec*FeoC is much more open and the β strands are shorter. Comparison of the structure of *kp*FeoC$_R$ to that of the winged-helix domain of DtxR (PDB ID: 1XCV) (D'Aquino et al. 2005) or the DNA binding domain of BlaI repressor (PBD ID: 1XSD) (Safo et al. 2005) showed that the B2 and B3 strands, as well as the W1 loop are much longer in *kp*FeoC$_R$. The winged-helix domain often uses helix-3 to bind to DNA and the DNA binding site often is highly positively charged, as is the case in BlaI repressor (Fig. 2e). In comparison, the corresponding helix-3 region in *kp*FeoC$_R$ is

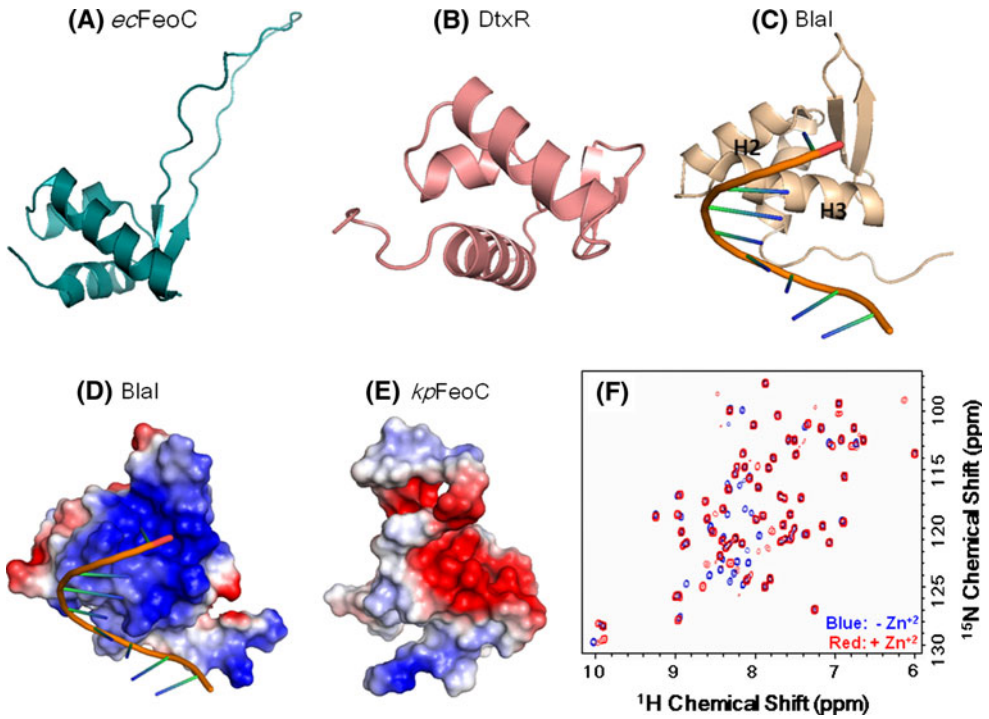

Fig. 2 **a** Ribbon representation of the structure of reduced FeoC from *E. coli* (*ec*FeoC$_R$). **b** Ribbon representation of the structure of the winged-helix domain of DtxR (PDB ID: 1XCV). **c** Ribbon representation of the structure of the DNA binding domain of BlaI repressor from *Staphylococus* aureus (PDB ID: 1XSD). The structure is shown in an orientation such that the DNA binding site is facing outward. **d** Surface charge distribution of the DNA binding domain of BlaI repressor. The orientation of the structure is the same as shown on (**c**). **e** Surface charge distribution of *kp*FeoC$_R$. The orientation of the H3 helix of *kp*FeoC$_R$ is the same as that in BlaI repressor shown in (**c**). **f** ^{1}H-^{15}N HSQC spectra of *kp*FeoC$_R$ without (*blue*) or in the presence of 1:1 molar ratio of Zn^{2+} (*red*). The surface charge distribution was generated with the program Pymol (The PyMOL Molecular Graphics System, Version 1.2r3pre, Schrödinger, LLC)

actually highly negatively charged, thus is unfavorable for interaction with the negatively charged DNA. This is consistent with our inability to detect DNA binding for *kp*FeoC (unpublished observation). In comparison, the putative DNA binding surface of *ec*FeoC is less negatively charged because of the following two substitutions in helix-3: $Asp^{34} \rightarrow Asn^{34}$ and $Glu^{38} \rightarrow Gln^{38}$.

Is FeoC a novel transcriptional regulator for feoABC ?

The *kp*FeoC has been proposed to be a [Fe–S]-dependent transcriptional regulator directly controlling the expression of the *feo* operon (Cartron et al. 2006) we next tested the metal cation binding affinity of $kpFeoC_R$. We found that it binds to Zn^{2+} (Fig. 2f). Binding of Zn^{2+} caused the disappearance of the resonances from the W1 loop region and minor changes of few resonances from residues near the W1 loop. Thus, Zn^{2+} is likely to bind to the cysteine residues in the W1 loop. In contrast, we could not detect any change in the ^{15}N-HSQC spectrum of $kpFeoC_R$ at 1:1 molar ratio of Fe^{2+}, (unpublished observation). Addition of Zn^{2+} or Fe^{2+} did not enhance the DNA binding affinity of *kp*FeoC (unpublished observation). Our results do not rule out the possibility that *kp*FeoC forms [Fe–S]-cluster in vivo since [Fe–S]-cluster is known to be highly unstable and that formation of [Fe–S]-cluster requires a biosynthetic machinery (Crack et al. 2012; Johnson et al. 2005). One best characterized sensory protein that requires the [Fe–S]-cluster is that of the *E. coli* O_2-sensing fumarate and nitrate reduction (FNR) regulator. The *E. coli* FNR becomes activated by insertion of an O_2-labile [4Fe–4S]-cluster into the N-terminal sensory domain by the iron-sulfur cluster (Isc) biosynthetic machinery. This causes conformational changes resulting in dimerization of the FNR monomer. This enables the C-terminal DNA-binding domain to recognize specific binding site within FNR-controlled promoters to regulate an array of >300 genes. The $kpFeoC_R$ protein in the present study is in the apo-from and it is still not clear whether the four cysteines in *kp*FeoC can form a [Fe–S]-cluster, thus its role as a [Fe–S]-dependent transcriptional regulator needs further examination.

Acknowledgments This work was supported by a grant (NSC 100-2311-B-001-023) from The National Science Council of the Republic of China. The NMR experiments were carried out with NMR spectrometers of the High-Field Nuclear Magnetic Resonance Center (HFNMRC) supported by National Research Program for Genomic Medicine, The National Science Council of the Republic of China.

References

Andrews SC, Robinson AK, Rodriguez-Quinones F (2003) Bacterial iron homeostasis. FEMS Microbiol Rev 27:215–237

Cartron ML, Maddocks S, Gillingham P, Craven CJ, Andrews SC (2006) Feo—transport of ferrous iron into bacteria. Biometals 19:143–157

Cornilescu G, Delaglio F, Bax A (1999) Protein backbone angle restraints from searching a database for chemical shift and sequence homology. J Biomol NMR 13:289–302

Crack JC, Green J, Hutchings MI, Thomson AJ, Le Brun NE (2012) Bacterial Iron–Sulfur Regulatory Proteins As Biological Sensor-Switches. *Antioxid Redox Signal* (on line March 6, 2012)

D'Aquino JA, Tetenbaum-Novatt J, White A, Berkovitch F, Ringe D (2005) Mechanism of metal ion activation of the diphtheria toxin repressor DtxR. Proc Natl Acad Sci U S A 102:18408–18413

Guilfoyle A, Maher MJ, Rapp M, Clarke R, Harrop S, Jormakka K (2009) Structural basis of GDP release and gating in G protein coupled Fe2 + transport. EMBO J 28:2677–2685

Hantke K (1987) Ferrous iron transport mutants in *Escherichia coli* K12. FEMS Microbiol Lett 44:53–57

Hung K-W, Chang Y-W, Eng ET, Chen J-H, Chen Y-C, Sun Y-J, Hsiao C-D, Dong G, Spasov KA, Unger VM, Huang T-H (2010) Structural fold, conservation and Fe(II) binding of the intracellular domain of prokaryote FeoB. J Struct Biol 170:501–512

Johnson DC, Dean DR, Smith AD, Johnson MK (2005) Structure, function, and formation of biological iron-sulfer cluster. Annu Rev Biochem 74:247–281

Kammler M, Schon C, Hantke K (1993) Characterization of the ferrous iron uptake system of *Escherichia coli*. J Bacteriol 175: 6212–6219

Koradi R, Billeter M, Wuthrich K (1996) MOLMOL: a program for display and analysis of macromolecular structures. J Mol Graphics 14:51–55

Laskowski RA, Rullmann JAC, MacArthur MW, Kaptein R, Thornton JM (1996) AQUA and PROCHECK—NMR: programs for checking the quality of protein structures solved by NMR. J Biomol NMR 8:477–486

Linge JP, O'Donoghue SI, Nilges M (2001) Automated assignment of ambiguous nuclear overhauser effects with ARIA. Methods Enzymol 339:71–90

Markley JL, Bax A, Arata Y, Hilbers CW, Kaptein R, Sykes BD, Wright PE, Wuthrich K (1998) Recommendations for the presentation of NMR structures of proteins and nucleic acids. IUPAC-IUBMB-IUPAB inter-union task group on the standardization of data bases of protein and nucleic acid structures determined by NMR spectroscopy. J Biomol NMR 12:1–23

Robey M, Cianciotto NP (2002) Legionella pneumophila feoAB promotes ferrous iron uptake and intracellular infection. Infect Immun 70:5659–5669

Safo MK, Zhao Q, Ko T-P, Musayev FN, Robinson H, Scarsdale N, Wang AH-J, Archer GL (2005) Crystal structures of the BlaI repressor from *Staphylococcus aureus* and its complex with DNA: insights into transcriptional regulation of the bla and mec operons. J Bacteriol 187:1833–1844

Stojiljkovic I, Cobeljic M, Hantke K (1993) Escherichia coli K-12 ferrous iron uptake mutants are impaired in their ability to colonize the mouse intestine. FEMS Microbiol Lett 108:111

Touati D (2000) Iron and oxidative stress in bacteria. Arch Biochem Biophys 373:1–6

Tsolis RM, Baumler AJ, Heffron F, Stojiljkovic I (1996) Contribution of TonB- and Feo-mediated iron uptake to growth of *Salmonella typhimurium* in the mouse. Infect Immun 64:4549–4556

Velayudhan J, Hughes NJ, McColm AA, Bagshaw J, Clayton CL, Andrews SC, Kelly DJ (2000) Iron acquisition and virulence in *Helicobacter pylori*: a major role for FeoB, a high-affinity ferrous iron transporter. Mol Microbiol 37:274–286

Wishart DS, Sykes BD (1994) Chemical shifts as a tool for structure determination. Methods Enzymol 239:363–392